Crystallographic and Electrochemical Characteristics of $La_{0.7}Mg_{0.3}Ni_{5.0-x}(Al_{0.5}Mo_{0.5})_x$ Hydrogen-Storage Alloys**

Xin Bo Zhang,[a] Dan Zi Sun,[b] Wen Ya Yin,[a] Yu Jun Chai,[a] and Min Shou Zhao*[a]

The structure, hydrogen-storage property and electrochemical characteristics of $La_{0.7}Mg_{0.3}Ni_{5.0-x}(Al_{0.5}Mo_{0.5})_x$ ($x=0$–0.8) hydrogen-storage alloys have been studied systematically. X-ray diffraction Rietveld analysis shows that all the alloys consist of an La (La,Mg)$_2$Ni$_9$ phase and an LaNi$_5$ phase. The pressure–composition isotherms indicate that the hydrogen-storage capacity first increases and then decreases with increasing x, and the equilibrium pressure decreases with increasing x. Electrochemical measurements show that the maximum discharge capacity and the exchange-current density of the alloy electrodes increase as x increases from 0 to 0.6 and then decrease when x increases further from 0.6 to 0.8. Moreover, the low-temperature dischargeability of the alloy electrodes increases monotonically with increasing x in the alloys.

1. Introduction

Hydrogen-storage alloys have been successfully used as negative electrode materials in the nickel–metal hydride battery (Ni–MH).[1–3] Besides the merits of higher energy density, higher charge and discharge ability, and longer charge/discharge cyclic life, the Ni–MH battery also has a smaller memory effect and causes less environmental pollution compared with the rechargeable nickel–cadmium battery.[4–6]

To date, almost all commercial Ni–MH batteries employ AB$_5$-type alloys as negative electrode materials because of their good overall electrode properties.[7] However, they are not yet satisfactory due to their limited discharge capacity.[8] A search for new types of hydrogen-storage-electrode alloys with higher energy density, rapid activation, high-rate dischargeability, long cyclic life and low cost to replace the conventional hydrogen-storage alloys, especially the earth-based AB$_5$-type alloys, is underway.[9]

Kadir et al.[10–12] reported that RMg$_2$Ni$_9$ (R: rare earth, Ca, Y) alloys with PuNi$_3$-type structures can absorb/desorb 1.8–1.87 wt.% H$_2$ and are thus promising candidates for reversible gaseous-hydrogen storage.[13, 14] The electrochemical properties and structures of LaCaMg(Ni,M)$_9$ (M = Al, Mn) alloys were studied by Chen et al.[6] Almost at the same time, Kohno et al.[3] reported that the discharge capacity of the La$_{0.7}$Mg$_{0.3}$Ni$_{2.8}$Co$_{0.5}$ alloy reached 410 mAh g^{-1}. However, up to now, the La–Mg–Ni–Co hydrogen-storage alloys cannot be used as negative electrode material for Ni–MH secondary batteries due to their serious corrosion in KOH electrolyte;[15] hence their cyclic stability must be upgraded for practical applications. In commercial AB$_5$-type alloys, the presence of 10 wt.% of Co has indeed improved the cyclic life of Ni–MH batteries. However, it deteriorates the discharge capacity, as well as the initial activation, and also constitutes about 40% of the material cost.[15] Numerous studies have been directed to find a more cost-effective substitute element, with a high reliability, to improve the cyclic life of Ni–MH batteries. It is believed that Al is one of the best candidates for cobalt substitution.[17] However, Al addition is detrimental to hydrogen diffusion from the electrode surface to the alloy bulk and thus inevitably decreases the high-rate discharge of the alloy electrodes.[2] It is reported that Mo addition can remarkably increase the kinetic property[18] as well as the electrochemical capacity of alloy electrodes.[19] Therefore, it can be expected that the overall electrochemical properties of the La–Mg–Ni–Co-type hydrogen-storage alloys could be improved by substitution of Al and Mo for Ni in the alloys.

Here, on the basis of our previous studies and the belief that the Al and Mo addition may result in some noticeable modification, the structure and electrochemical characteristics of the $La_{0.7}Mg_{0.3}Ni_{5.0-x}(Al_{0.5}Mo_{0.5})_x$ ($x=0$–0.8) hydrogen-storage alloys have been systematically investigated.

Experimental Section

Alloy Preparation and Structure Analyses: All alloy samples were prepared by arc-melting constituent metals with purities above 99% under argon atmosphere on a water-cooled copper hearth. To ensure good homogeneity of the alloys, ingots were turned over and remelted five times. A slight excess of Mg was needed to compensate for evaporative loss of Mg under preparation condi-

[a] Dr. X. B. Zhang, W. Y. Yin, Y. J. Chai, Prof. M. S. Zhao
Key Laboratory of Rare Earth Chemistry and Physics
Changchun Institute of Applied Chemistry, Chinese Academy of Sciences
5625 Remin Street, Changchun 130022 (P. R. China)
Fax: (+86) 431-569-8041
E-mail: eboat@ciac.jl.cn

[b] Dr. D. Z. Sun
State Key Laboratory of Electroanalytical Chemistry
Changchun Institute of Applied Chemistry, Chinese Academy of Sciences
5625 Remin Street, Changchun 130022 (P. R. China)

[**] $x=0$–0.8

tions. Thereafter, these alloy samples were mechanically crushed into fine powders of 200–300 mesh in a mortar. The final alloys were carefully checked by inductively coupled plasma-atomic emission spectrometry (ICP-AES) using a TJA Poems-type instrument.

The crystal structure was determined by X-ray diffraction on a Rigaku D/Max 2500PC X-ray diffractometer (CuK_α radiation, Bragg–Brentano geometry, 2θ range 10–100°, step size 0.02°, 4 s per step, backscattered rear graphite monochromator) using the JADE5 software.[20] The phase abundance and the lattice parameter were calculated by means of the RIETICA program.

Electrochemical Measurements: Electrodes of different alloys were prepared by mixing 0.15 g alloy powder with 0.75 g nickel carbonyl powder to uniformity and then cold-pressing the material into a pellet, which had a diameter of 13 mm and a thickness of 1.5 mm. Electrochemical measurements were performed in a standard open three-electrode cell that consisted of a working electrode (metal hydride electrode), a counter electrode (NiOOH/Ni(OH)$_2$ electrode), and a reference electrode (Hg/HgO electrode). The electrolyte in the cell was a 6 M KOH aqueous solution. Charge and discharge tests were carried out on an automatic galvanostatic system (DC-5). Each electrode was charged at 60 mA g^{-1} for 7 h followed by a 30 min rest and then discharged at the same discharge current density to the cutoff voltage of −0.60 V versus Hg/HgO. For investigation of the high-rate dischargeability, the discharge capacities at various discharge-current densities were measured.

Pressure–composition isotherms (P–C–T) were electrochemically obtained by converting the equilibrium potential of the metal-hydride electrode to the equilibrium pressure of hydrogen on the basis of the Nernst equation using electrochemical data[21] as reported in ref. [22].

The linear polarisation curves of the alloy electrodes were measured by scanning the electrode potential at the rate of 0.1 mV s^{-1} from −5 to 5 mV (versus open circuit potential) at 50% depth of discharge at 298 K and 233 K, respectively. The polarisation resistance R_p was obtained from the slope of the linear polarisation curves. Then, the exchange-current density I_0 was calculated from the value of R_p from Equation (1).[16]

$$I_0 = \frac{RT}{FR_p} \tag{1}$$

where R is the gas constant; T is the absolute temperature; F is the Faraday constant. For the potentiostatic discharge, the test electrodes in the fully charged state were discharged following a + 500 mV potential step for 500 s. Both the linear polarisation curves and the potentiostatic discharge were measured on an EG&G PARC Model 273 Potentiostat/Galvanostat.

2. Results and Discussion

2.1 Alloy Composition and Structure Characteristics

Low-melting Mg metal is known to be inevitably lost during the sample preparation by arc-melting. Numerous studies have been made to overcome this problem, such as using a Mg–Ni master alloy as a Mg additive, decreasing the melting current,

adding a slight excess of Mg over sample composition, and so on. Among all these methods, we find that the third is the most effective way to compensate evaporative loss of Mg. Several attempts were made until the optimum preparative conditions were found. Herein, the lost weight during sample preparation is almost the same as the excess Mg added. The results of ICP-AES analysis for all compounds are given in Table 1. It can be seen that the final composition of all the alloys is identical to the target composition.

Table 1. Chemical composition of the La$_{0.7}$Mg$_{0.3}$Ni$_{5.0-x}$(Al$_{0.5}$Mo$_{0.5}$)$_x$ (x = 0–0.8) alloys.

Sample	La [mg g^{-1}]	Mg [mg g^{-1}]	Ni [mg g^{-1}]	Al [mg g^{-1}]	Mo [mg g^{-1}]	La : Mg : Ni : Al : Mo[a]
$x=0.0$	244.30	18.32	737.38	0.00	0.00	1.76 : 0.75 : 12.56 : 0 : 0
$x=0.2$	243.96	18.30	706.91	6.77	24.07	1.76 : 0.75 : 12.04 : 0.25 : 0.25
$x=0.4$	243.62	18.27	676.51	13.52	48.07	1.75 : 0.75 : 11.52 : 0.50 : 0.50
$x=0.6$	243.28	18.25	646.21	20.25	72.01	1.75 : 0.75 : 11.01 : 0.75 : 0.75
$x=0.8$	242.95	18.22	615.98	26.96	95.88	1.75 : 0.75 : 10.49 : 1.00 : 1.00

[a] Atomic ratio.

The XRD and Rietveld analysis patterns for the La$_{0.7}$Mg$_{0.3}$Ni$_{4.8}$-(Al$_{0.5}$Mo$_{0.5}$)$_{0.2}$ hydrogen-storage alloy, given as an example of the La$_{0.7}$Mg$_{0.3}$Ni$_{5.0-x}$(Al$_{0.5}$Mo$_{0.5}$)$_x$ (x = 0–0.8) hydrogen-storage alloys, are shown in Figure 1. It can be seen that the alloy
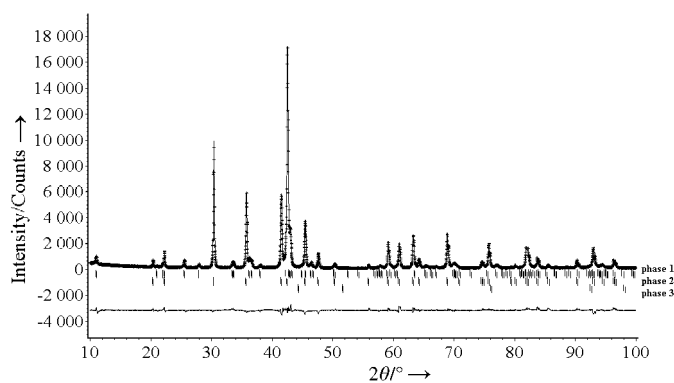

Figure 1. Rietveld refinement of the XRD profiles for the La$_{0.7}$Mg$_{0.3}$Ni$_{4.8}$(Al$_{0.5}$Mo$_{0.5}$)$_{0.2}$ hydrogen-storage alloy (Phase 1: La(La,Mg)$_2$Ni$_9$; phase 2: LaNi$_5$; phase 3: Ni).

mainly consists of an La$_2$MgNi$_9$ phase with a PuNi$_3$-type rhombohedral structure and an LaNi$_5$ phase with a CaCu$_5$-type hexagonal structure. The final Rietveld structure parameter of the La$_2$MgNi$_9$ phase is tabulated in Table 2. It should be noted that La atoms in La$_2$MgNi$_9$ are located not only at the 3a site (the Pu1 atom position of the PuNi$_3$ structure), but also at the 6c sites (the Pu2 atom position of the PuNi$_3$ structure), while Mg atoms in the alloy exhibit a strong preference for the 6c sites. The final structure of La$_2$MgNi$_9$ phase can thus be designated as La(La,Mg)$_2$Ni$_9$. The phase abundance and lattice parameter of various phases of the La$_{0.7}$Mg$_{0.3}$Ni$_{5.0-x}$(Al$_{0.5}$Mo$_{0.5}$)$_x$ (x = 0–0.8) hydrogen-storage alloys are listed in Table 3. It can be found that all the alloys consisted of an impurity Ni phase and two main crystallographic phases, namely the La(La,Mg)$_2$Ni$_9$ phase

Table 2. Crystallographic parameters for La_2MgNi_9 using X-ray diffraction Cu Kα_1 ($\lambda = 1.5405981$ Å) at 298 K in a space group R−3m and Z=3[a].

Atom	Site	Metal atom position			Occupancy
		x	y	z	
La1	3a	0	0	0	1
La2	6c	0	0	0.1428(2)	0.478
мg1	6c	0	0	0.1428(2)	0.522
Ni1	6c	0	0	0.3310(3)	1
Ni2	3b	0	0	0.5	1
Ni3	18h	0.4995(1)	0.5005(1)	0.0855(2)	1

[a] Structure was refined using the Rietveld refinement program Rietica. The pattern factor $R_p = 5.6$, the weighted pattern factor $R_{wp} = 7.5$ and the goodness-of-fit $S = 1.8$.

Table 3. Characteristics of alloy phases in $La_{0.7}Mg_{0.3}Ni_{5.0-x}(Al_{0.5}Mo_{0.5})_x$ (x=0–0.8) alloys.

Sample	Phase	Phase Abundance [wt.%]	Lattice Parameter [Å] a		Cell Volume [Å] c
	La(La,Mg)$_2$Ni$_9$	29.13	4.968	23.991	512.79
x=0.0	LaNi$_5$	70.17	5.042	4.008	88.24
	Ni	0.70	3.520	3.520	43.61
	La(La,Mg)$_2$Ni$_9$	27.38	4.992	24.266	523.7
x=0.2	LaNi$_5$	72.18	5.051	4.025	88.93
	Ni	0.43	3.531	3.531	44.02
	La(La,Mg)$_2$Ni$_9$	24.95	5.022	24.308	530.93
x=0.4	LaNi$_5$	74.69	5.056	4.028	89.17
	Ni	0.36	3.534	3.534	44.14
	La(La,Mg)$_2$Ni$_9$	24.33	5.055	24.519	542.6
x=0.6	LaNi$_5$	75.39	5.069	4.053	90.19
	Ni	0.28	3.547	3.547	44.63
	La(La,Mg)$_2$Ni$_9$	22.13	5.103	24.609	554.98
x=0.8	LaNi$_5$	77.58	5.075	4.061	90.58
	Ni	0.28	3.559	3.559	45.08

Figure 2. Cell parameter and volume as a function of x in $La_{0.7}Mg_{0.3}Ni_{5.0-x}$ $(Al_{0.5}Mo_{0.5})_x$ alloys (x=0–0.8): (top) La(La,Mg)$_2$Ni$_9$ phase; (bottom) LaNi$_5$ phase.
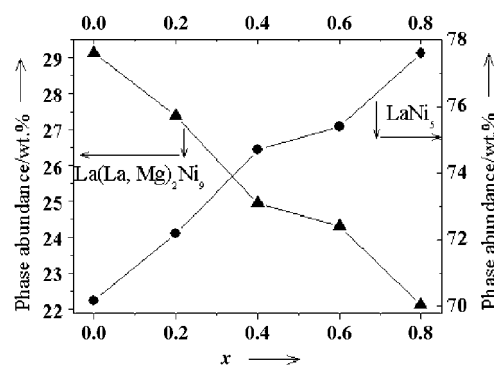
Figure 3. Variation of phase abundance of the La(La,Mg)$_2$Ni$_9$ and LaNi$_5$ phases in the $La_{0.7}Mg_{0.3}Ni_{5.0-x}(Al_{0.5}Mo_{0.5})_x$ (x=0–0.8) alloys.
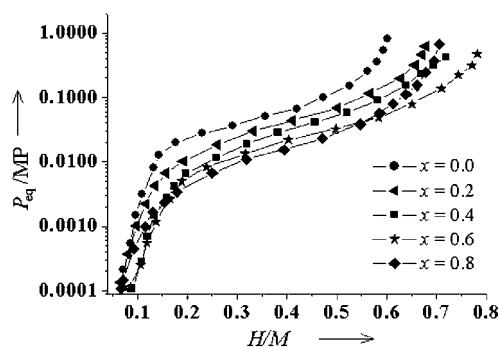
Figure 4. Electrochemical P–C–T curves for $La_{0.7}Mg_{0.3}Ni_{5.0-x}(Al_{0.5}Mo_{0.5})_x$ alloy electrodes at 298 K.

and the LaNi$_5$ phase. Figure 2 shows the lattice parameter and unit-cell volume of the two main phases as a function of *x* in the alloys. It can be seen that *a*, *c* and the cell volumes of both the La(La,Mg)$_2$Ni$_9$ phase and the LaNi$_5$ phase increase monotonically with increasing *x* in the alloys. This is mainly ascribed to the fact that the atomic radii of Al (1.432 Å) and Mo (1.363 Å) are larger than that of Ni (1.246 Å). The relationship between the phase abundance of the La(La,Mg)$_2$Ni$_9$ phase and the LaNi$_5$ phase and *x* in the alloys is shown in Figure 3. It can be seen that, with the increase of *x* in the alloys, the La(La,Mg)$_2$Ni$_9$ phase abundance decreases from 29.13% to 22.13%; on the contrary, the LaNi$_5$ phase abundance increases from 70.17% to 77.58%. These results influence the hydrogen-storage and electrochemical characteristics of the alloys studied.

2.2 P–C Isotherms

Figure 4 shows the electrochemical P–C–T curves for the $La_{0.7}Mg_{0.3}Ni_{5.0-x}(Al_{0.5}Mo_{0.5})_x$ (x=0–0.8) alloy electrodes at 298 K. It can be seen that the desorption pressure reduces continually as the Al and Mo additions increase. This means that the stabil-
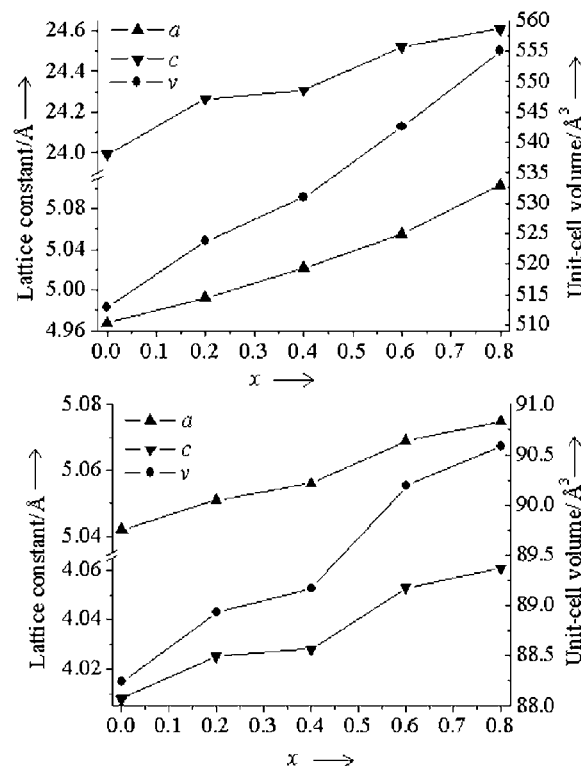
ity of the hydrides of alloys increases with increasing Al and Mo content due to the larger unit-cell volume of the alloy. This phenomenon is consistent with those reported previously for AB_3 alloys[14] and most AB_5 alloys.[23] Moreover, it can be seen that there is only one quasiplateau region in each P–C–T curve, as shown in Figure 4. The unit cells of the AB_3 compounds contain one-third AB_5 structure and two-thirds AB_2 structure,[6] so it is possible that the plateau pressure of the $La(La,Mg)_2Ni_9$ phase is similar to that of the $LaNi_5$ phase, or that the difference between the plateau pressures of the AB_3 and AB_5 compounds is too small to be observed.

With the increase of Al and Mo contents in the alloys, the hydrogen-storage capacity first increases from 0.603 to 0.782, and then decreases to 0.706. This may be due to two reasons: As mentioned above, the plateau pressure decreases with increase of Al and Mo addition to the alloys, which enhances the intrinsic hydrogen-storage capacity of the alloys. On the other hand, it is known that the hydrogen-storage capacity of the La-$(La,Mg)_2Ni_9$ phase is larger than that of the $LaNi_5$ system alloy;[24] however, the $La(La,Mg)_2Ni_9$ phase abundance decreases with increasing x. Therefore, it is believed that there is an optimum Al and Mo content for improving the overall properties of the La–Mg–Ni–Al–Mo-type hydrogen-storage alloys. The recommended amount of Al and Mo addition is 0.6 from this work.

2.3 Discharge Capacity and Discharge Potential

The number of cycles needed to activate the electrodes, and the maximum discharge capacity of the $La_{0.7}Mg_{0.3}Ni_{5.0-x}$ $(Al_{0.5}Mo_{0.5})_x$ $(x = 0-0.8)$ alloy electrodes are listed in Table 4. It can be seen that all these alloys can be easily activated to

Table 4. *Electrode performance of $La_{0.7}Mg_{0.3}Ni_{5.0-x}(Al_{0.5}Mo_{0.5})_x$ $(x = 0-0.8)$ alloys.*

Sample	H/M	C_{max}[mAh g^{-1}]	N_a[a]	HRD_{1200}[b][%]	S_{70} [%]
$x = 0.0$	0.603	243.8	3	58.6	49.0
$x = 0.2$	0.678	273.7	3	61.4	53.2
$x = 0.4$	0.719	289.7	2	66.7	57.8
$x = 0.6$	0.782	314.6	2	74.2	63.0
$x = 0.8$	0.706	287.6	2	77.6	66.6

[a] The number of cycles needed to activate the electrodes. [b] The high-rate dischargeability at the discharge-current density of 1200 mA g^{-1}.

reach the maximum capacity within three cycles. In addition, the maximum discharge capacity of the alloy electrodes increases first and then decreases as x increases from 0 to 0.8. The maximum discharge capacity of the alloy electrodes reaches a maximum of 314.6 mAh g^{-1} when $x = 0.6$ and then decreases to 287.6 mAh g^{-1} when $x = 0.8$. The variation of maximum discharge capacity of the alloys is basically consistent with the variation of the H/M with the Al and Mo content in the alloys.

Figure 5 shows the discharge curves (fifth cycle) of the alloy electrodes at 60 mA g^{-1} and 298 K. Obviously each curve has a

wide discharge-potential plateau based on the oxidation of desorbed hydrogen from the hydride. Moreover, the discharge plateau shifts to the negative side as Al and Mo addition increases in the alloys. As shown in Figure 5, the mid-discharge (potential at 50% depth of discharge) potential decreases from -0.8721 to -0.8189 V when x increases from 0 to 0.8, which is in agreement with the reduction of the desorption plateau pressure with the increase of Al and Mo content in the alloys.
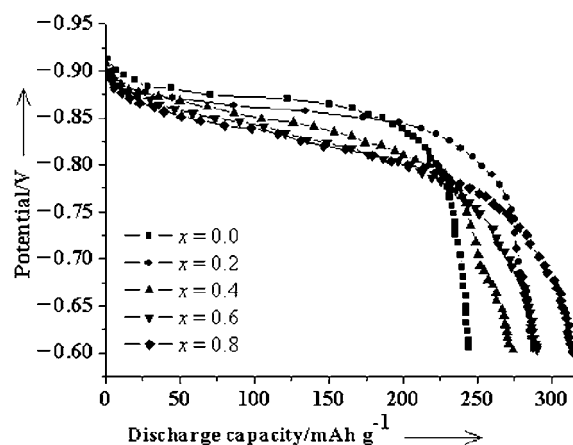

Figure 5. *Discharge curves of $La_{0.7}Mg_{0.3}Ni_{5.0-x}(Al_{0.5}Mo_{0.5})_x$ $(x = 0-0.8)$ alloy electrodes at a discharge current density of 60 mA g^{-1} and 298 K.*

2.4 Cyclic Stability

The cycling capacity retention rate, expressed as $S_{70}(\%) = C_{70}/C_{max} \times 100$ (where C_{max} is the maximum discharge capacity, C_{70} is the discharge capacity after 70 cycles), S_{70} at 60 mA g^{-1} is also listed in Table 4. It can be seen that S_{70} increases noticeably from 49.0 to 66.6% as x increases from 0 to 0.8, indicating that the cyclic stability of the La–Mg–Ni–Al–Mo-type alloys improves markedly with an increase in their Al and Mo content. It is known that the capacity degradation of La–Mg–Ni-type alloy electrodes results primarily from two factors: the corrosion of Mg and La elements and the pulverisation of the alloy particles.[23] Here, the improved cyclic stability may be due to the formation of a dense Al oxide (hydroxide) layer on the alloy surface, which subsequently provides the alloy with strong protection from further corrosion of La and Mg. Further investigations in this aspect are on-going.

2.5 High-Rate Dischargeability (HRD) and Electrochemical Kinetics

For hydride electrodes in batteries, it is very important to inhibit the decrease of the discharge capacity even at the high charge/discharge current density. Figure 6 shows the relationship between the high-rate dischargeability and the discharge current density of the $La_{0.7}Mg_{0.3}Ni_{5.0-x}(Al_{0.5}Mo_{0.5})_x$ $(x = 0-0.8)$ alloy electrodes. It can be seen that HRD of the alloy electrodes increases monotonously with increasing x. The HRD of the alloy electrodes for the discharge current density of 1200 mA g^{-1} is also listed in Table 4. It can be seen that as x in-
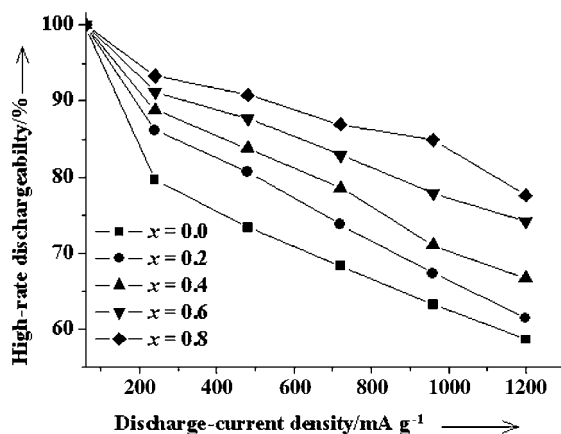
Figure 6. High-rate dischargeability of $La_{0.7}Mg_{0.3}Ni_{5.0-x}(Al_{0.5}Mo_{0.5})_x$ alloy electrodes at 298 K.

creases, the HRD of the alloy electrodes increases from 58.6 % ($x=0$) to 77.6 % ($x=0.8$). It is well-known that the HRD values of metal-hydride electrodes are influenced mainly by the electrochemical reaction kinetics on the alloy powder surface and the diffusion rate of hydrogen in the bulk of the alloy.[25] The exchange-current density I_0 of the hydrogen-storage alloy electrodes is commonly used to characterise the catalytic activity for charge-transfer at the alloy electrode surface. When the overpotential is changed within a small range, the polarisation resistance R_p can be estimated from the slope of the linear polarisation curve. Then the I_0 is calculated from the value of R_p according to Equation (1). The obtained values of I_0 and R_p are summarised in Table 5. Figure 7 shows high-rate dischargeability as a function of I_0 for the hydrogen-evolution reaction at the alloy electrodes. It can be seen that the HRD is a linear function of I_0. Moreover, we find that the hydrogen diffusion coefficient D is almost unchanged (13.4–13.9×10^{-10} cm^2 s^{-1}). Iwakura et al.[26] have shown that, if the electrochemical reaction on the surface is the rate-determining factor, a linear dependence of the high-rate dischargeability on the exchange-
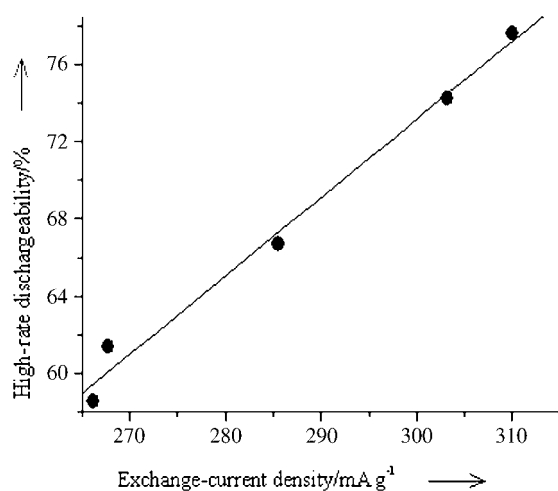
Table 5. Electrochemical kinetic parameters of $La_{0.7}Mg_{0.3}Ni_{5.0-x}(Al_{0.5}Mo_{0.5})_x$ ($x=0$–0.8) alloy electrodes.

sample	Polarization resistance, R_p [mΩ]		Exchange-current density, I_0 [mA g^{-1}]		Hydrogen-diffusion coefficient D [$\times 10^{-10}$ cm^{2}s^{-1}]	
	298 K	233 K	298 K	233 K	298 K	233 K
$x=0.0$	86.32	240.99	266.23	83.21	13.4	1.7
$x=0.2$	85.81	239.72	267.8	83.65	13.5	3.2
$x=0.4$	80.5	238.81	285.5	83.97	13.8	3.9
$x=0.6$	75.81	238.32	303.15	84.14	13.9	5.1
$x=0.8$	74.14	237.62	310	84.39	13.9	6.5

current density should be observed. In contrast, if the diffusion of hydrogen in the bulk is the rate-determining factor, the high-rate dischargeability should be constant, irrespective of exchange density. Therefore, herein, the HRD is essentially controlled by the charge-transfer reaction of hydrogen on the surface at a discharge-current density of 1200 mA g^{-1}.

2.6 Low-Temperature Dischargeability

It has been reported that the conventional nickel–metal battery exhibits a poor low-temperature dischargeability (LTD).[27] Sakai et al.[2] pointed out that the dischargeability of the negative electrodes at relatively low temperatures depended on hydrogen diffusion and/or charge-transfer process occurring at the metal/electrolyte interface. The D of hydrogen in the bulk is evaluated using the method described by Iwakura et al.[18] The LTD, expressed as LTD$_{233}$(%) $= C_{233}/C_{298} \times 100$ (where C_{233} and C_{298} are the discharge capacity at 233 K and 298 K, respectively). The D and the I_0 of the $La_{0.7}Mg_{0.3}Ni_{5.0-x}(Al_{0.5}Mo_{0.5})_x$ ($x=0$–0.8) alloy electrodes at 233 K are also listed in Table 5. It can be found that both the I_0 and the D are smaller than that at 298 K. However, the D is much larger than that of other alloys[28] even at low temperature, indicating the $La_{0.7}Mg_{0.3}Ni_{5.0-x}(Al_{0.5}Mo_{0.5})_x$ alloys aid hydrogen diffusion. Meanwhile, we can find that the I_0 remains almost unchanged (83.21–84.39 mA g^{-1}); whereas the D increases remarkably with increasing x, which implies that the hydrogen diffusion in the alloy probably becomes the rate-determining factor for low-temperature dischargeability at 233 K. Figure 8 shows the LTD as a function of D in the alloy electrodes. It can be easily found that the D increases with the increases of x, which can be attributed to the cell-volume expansion, as shown in Table 3. The increasing D accordingly increases the LTD of the alloy electrodes.

3. Conclusions

The structure, hydrogen-storage characteristics and electrochemical properties of the $La_{0.7}Mg_{0.3}Ni_{5.0-x}(Al_{0.5}Mo_{0.5})_x$ ($x=0$–0.8) hydrogen-storage alloys were investigated systematically. The X-ray powder diffraction and Rietveld analysis reveal that all the alloys consist of an impurity Ni phase and two main crystallographic phases, namely La(La,Mg)$_2$Ni$_9$ and LaNi$_5$, and that the lattice parameters and cell volumes of both the La(La,Mg)$_2$Ni$_9$ and LaNi$_5$ phases increase with increasing Al and Mo con-

Figure 7. High-rate dischargeability as a function of exchange-current density for the hydrogen-evolution reaction at $La_{0.7}Mg_{0.3}Ni_{5.0-x}(Al_{0.5}Mo_{0.5})_x$ alloy electrodes.
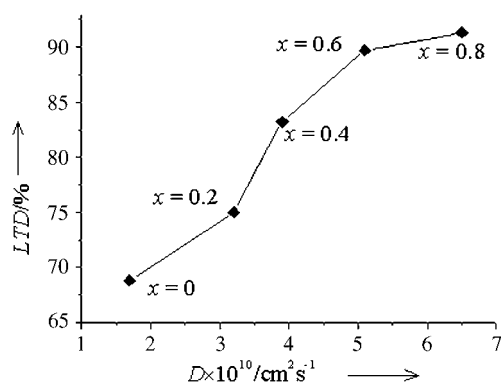
Figure 8. *Low-temperature dischargeability (LTD) as a function of the hydrogen diffusion coefficient for $La_{0.7}Mg_{0.3}Ni_{5.0-x}(Al_{0.5}Mo_{0.5})_x$ alloy electrodes at 233 K.*

tent. The P–C–T curves indicate that the hydrogen-storage capacity first increases and then decreases, and that the plateau pressure decreases with increasing x. The electrochemical measurements show that the maximum discharge capacity increases from 243.8 ($x=0$) to 314.6 mAh g^{-1} ($x=0.6$) and then decreases to 256.4 mAh g^{-1} ($x=0.8$). For the discharge current density of 1200 mA g^{-1}, the high-rate dischargeability of the alloy electrodes increases progressively from 58.6% ($x=0$) to 77.6% ($x=0.8$). The hydrogen-diffusion coefficient increases with increasing Al and Mo content, and thus increases the low-temperature dischargeability of the alloy electrodes.

Acknowledgements

[1] H. G. Pan, Y. F. Zhu, M. X. Gao, Q. D. Wang, *J. Electrochem. Soc.* **2002**, *149*, A829–A833.
[2] T. Sakai, H. Miyamura, N. Kuriyama, A. Kato, K. Oguro, H. Ishikawa, *J. Electrochem. Soc.* **1990**, *137*, 795–799.
[3] T. Kohno, H. Yoshida, F. Kawashima, T. Inaba, I. Sakai, M. Yamamoto, M. Kanda, *J. Alloys Compd.* **2000**, *311*, L5–L7.
[4] J. J. G. Willems, *Philips J. Res.* **1984**, *39 (Suppl. 1)*, 1–94.
[5] J. J. G. Willems, K. H. J. Buschow, *J. Less-Common Met.* **1987**, *129*, 13–30.
[6] J. Chen, N. Kuriyama, H. T. Takeshita, H. Tanaka, T. Sakai, M. Haruta, *Electrochem. Solid-State Lett.* **2000**, *3*, 249–252.
[7] T. Sakai, I. Uehara, H. Iwakura, *J. Alloys Compd.* **1999**, *293–295*, 762–769.
[8] J. J. Reilly, G. D. Adzic, J. R. Johnson, T. Vogt, S. Mukerjee, J. McBreen, *J. Alloys Compd.* **1999**, *293–295*, 569–582.
[9] Y. F Liu, H. G. Pan, Y. F. Zhu, R. Li, Y. Q. Lei, *Mater. Sci. Eng., A* **2004**, *372*, 163–172.
[10] K. Kadir, T. Sakai, I. Uahara, *J. Alloys Compd.* **1997**, *257*, 115–121.
[11] K. Kadir, N. Nuriyama, T. Sakai, I. Uehara, L. Eriksson, *J. Alloys Compd.* **1999**, *284*, 145–154.
[12] K. Kadir, T. Sakai, I. Uahara, *J. Alloys Compd.* **1999**, *287*, 264–270.
[13] K. Kadir, T. Sakai, I. Uahara, *J. Alloys Compd.* **2000**, *302*, 112–117.
[14] J. Chen, H. T. Takeshita, H. Tanaka, N. Kuriyama, T. Sakai, *J. Alloys Compd.* **2000**, *302*, 304–313.
[15] B. Liao, Y. Q. Lei, L. X. Chen, G. L. Lu, H. G. Pan, Q. D. Wang, *J. Power Sources* **2004**, *129*, 358–367.
[16] P. H. Notton, P. Hokkeling, *J. Electrochem. Soc.* **1991**, *138*, 1877–1885.
[17] T. Sakai, H. Miyamura, N. Kuriyama, A. Kato, K. Oguro, H. Ishikawa, *J. Less-Common Met.*, **1990**, *159*, 127–139.
[18] C. Iwakura, H. Senoh, K. Morimoto, Y. Hara, H. Inoue, *Electrochem.* **2002**, *70*, 2–7.
[19] M. T. Yeh, V. M. Beibutian, S. E. Hsu, *J. Alloys Compd.* **1999**, *293–295*, 721–723.
[20] Materials Data JADE Realease 5, XRD pattern processing, Materials Data Inc. (MDI), **1997**.
[21] T. Sakai, K. Oguro, H. Miyamura, N. Kuriyama, A. Kato, H. Ishikawa, C. Iwakura, *J. Less-Common Met.* **1990**, *161*, 193–202.
[22] H. G. Pan, Q. W. Jin, M. X. Gao, Y. F. Liu, R. Li, Y. Q. Lei, *J. Alloys Compd.* **2004**, *373*, 237–245.
[23] J. J. Reilly in *Handbook of Battery Materials* (Ed.: J. O. Bessenhard), Wiley, New York, **2000**.
[24] H. G. Pan, Y. F. Liu, M. X. Gao, Y. Q. Lei, Q. D. Wang, *J. Electrochem. Soc.* **2003**, *150*, A565–A570.
[25] T. Sakai, H. Miyamura, N. Kuriyama, A. Kato, K. Oguro, H. Ishikawa, *J. Less-Common Met.* **1990**, *159*, 127–139.
[26] C. Iwakura, T. Oura, H. Inoue, M. Matsuoka, *Electrochim. Acta* **1996**, *41*, 117–121.
[27] H. Senoh, Y. Hara, H. Inoue, C. Iwakura, *Electrochim. Acta* **2001**, *46*, 967–971.
[28] Y. F. Liu, H. G. Pan, Y. F. Zhu, R. Li, Y. Q. Lei, *Mater. Sci. Eng., A* **2004**, *372*, 163–172.